PNAS
www.pnas.org

Supplementary Information for

The molecular mechanism of fusion pore formation driven by the neuronal SNARE complex

Satyan Sharma and Manfred Lindau

Satyan Sharma
Email: satyan.sharma@mpibpc.mpg.de

This PDF file includes:

- Supplementary Information Text
- Figs. S1 to S8
- Tables S1 to S2
- Captions for movies S1
- References for SI reference citations

Other supplementary materials for this manuscript include the following:

- Movies S1

www.pnas.org/cgi/doi/10.1073/pnas.1816495115

Supplementary Information Text

Supporting Methods

Generation of partially unzipped SNARE models

The initial SNARE complex structure was taken from PDB entry 3HD7 [1]. The missing C-terminal residues T116 of Syb2, F287-G288 of Stx1, and K201-G206 of SNAP-25 were added using Modeller [2]. The SNAP-25 linker region residues K83 to A100 (KFCGLCVCPCNKLKSSDA) were added assigning a random coil secondary structure, as predicted by I-TASSER server [3]. The atomistic structures of syb2 and of the stx1/SNAP-25 t-SNARE complex were separately converted to coarse-grain models using the standard "martinize" script (http://www.cgmartini.nl/) and reassembled to the original SNARE complex. Following the conversion of atomistic SNARE complex to CG model, the palmitoyl chains were added to SNAP-25 residues C85, C88, C90 and C92, based on the lipid tail definition for the DPPC CG model. The CG model of the SNARE complex was placed in a cubic box of 19.2 nm^3, solvated with CG water, charge neutralized and energy minimized. The SNARE domains were then partially unzipped by pulling T116 of syb2 away from G288 of stx1 at a constant pulling rate of 0.2 nm/ns using a force constant of 100 kJ mol^{-1} nm^{-2}. The unzipping simulation was stopped when the TM domains were separated and the pulled groups were 8.2 nm apart. The stx1 TM domain of the partially unzipped SNARE complex was then placed in a pre-equilibrated DPPC bilayer (box size 19.78 x 19.78 x 30.48 nm^3), and pulling was further continued, along the bilayer normal, until layer +5 was unzipped and the pulled groups were 13.9 nm apart.

Insertion of SNARE proteins in plasma membrane by self-assembly

The self-assembly of the planar plasma membrane[4] was carried out by randomly placing the extracellular (EC) and intracellular (IC) leaflet lipids into two separate 38 nm x 38 nm x 5 nm simulation boxes (see Supplementary Table S1, before self-assembly). The two boxes were then combined by placing the IC lipids box on top of EC box, with an overlap of 0.5 nm. The box was enlarged along the z-dimension and four copies of the SNARE complex placed in the resulting box (38 nm x 38 nm x 20 nm) with the partially zipped SNARE domains pointing radially away from each other. The protein was oriented such that EC lipids surrounded the C-terminus of stx1 and the palmitoylated chains of modified cysteines of SNAP-25 would be located in the IC lipids box. The resulting simulation box was filled with water and ions were added to achieve a final 0.10 M salt concentration. After initial rounds of energy minimizations, the lipids were then allowed to self-assemble into a bilayer over 500 ns. During the self-assembly, the entire syb2 protein along with SNARE domains of the stx1 and SNAP-25 proteins were position restrained along x- and y- directions.

Preparation of ND-lipid system

The ND scaffold protein was based on variant MSP1E2 of membrane scaffold protein 1 (MSP1)[5]. A structural model of MSP1E2 was generated by duplicating two of the amphipathic helices (H4-H5) into the crystal structure [PDB entry 1AV1] of the lipid-binding domain of ApoA-I[6]. To fill the ND with a patch of membrane with lipid composition based on synaptic vesicle (SV) lipid composition[7], the empty ND scaffold protein was placed above a pre-equilibrated SV planar bilayer[4]. The ND scaffold protein ring was then manually dragged into this asymmetric planar bilayer using VMD. The SV lipids located outside the circular ND and the lipids that clashed with the scaffold protein were removed, keeping only the lipids that were located inside the ND. The final lipid composition is given in Supplementary Table 2. Care was taken to ensure an equal lipid area in the two leaflets, based on our previous estimate of a 0.43-0.45 nm^2 area per lipid for such a multicomponent bilayer[4]. The lipid area was consistent with previous experimental[8] and computer simulation studies[9] that estimated a maximum number of 250 DMPC lipids in a MSP1E2 ND. The ND was subjected to a few rounds of energy minimization and a subsequent 2 μs equilibration.

Lipid tilt analysis

All analyses were done using GROMACS tools and self-written scripts. The trajectory frames were analyzed every 1 ns. The lipid tail contact analysis between the opposing membranes employed a cutoff of 0.5 nm. The lipid tilt was calculated only for phospholipids according to the scheme described previously[10]. Briefly, the tilt was calculated as the angle between an individual lipid orientation vector and the bilayer normal. The lipid orientation vector was defined as the vector connecting the geometric center of mass of phosphate and carbonyl beads of the fatty acids with the geometric center of mass of the terminal carbon beads of the two lipid tails.

Fusion pore conductance analysis

The conductance G_{pore} (pS) of simulated fusion pores was determined from their geometry using the relation[11].

$$G_{pore} = \frac{\gamma}{\left\{\sum_{z\ low}^{z\ high} \frac{s}{A(z)}\right\}} \qquad \text{(S1)}$$

where s is a slice width (s=0.45 nm) and γ is the bulk conductivity of the solution within the fusion pore (here $\gamma = 1.5 \times 10^3$ pS/nm). The cross-sectional areas (A(z)) of the fusion pore at given z coordinates were calculated based on the number of waters (n_w) in each slice and water bulk density (ρ_w) using the relation:

$$A(z) = \frac{n_w(z)}{\rho_w \cdot s} \qquad \text{(S2)}$$

The upper and lower bounds of the fusion pore (z high and z low) were defined using a 12 nm^2 cut-off, i.e., the slices with area greater than 12 nm^2 were considered to be occupied by bulk electrolyte. The cut-off was chosen based on visual inspections of the trajectories and water density profiles in the fusion pore along the z-direction.

For the simulations where continuous water densities traversing the membrane were identified for at least 25 ns, a corrected fusion pore conductance was also calculated by taking the reduced water self-diffusion inside the fusion pore into account[11]:

$$G_{pore}^{corr} = \frac{\gamma}{\left\{\sum_{z=low}^{z=high} \frac{D_z(bulk)s}{D_z(z)A(z)}\right\}} \qquad \text{(S3)}$$

where $D_z(z)$ is the average one-dimensional diffusion coefficient of water particles in each slice of the fusion pore at a given z- coordinate and D_z (bulk) is the one-dimensional diffusion coefficient of the bulk solvent along z-direction.

To obtain $D_z(z)$ the mean square displacement (MSD) of waters was calculated for each slab using the GROMACS utility g_msd, at 1 ns intervals, along the z-axis. The water beads located in a given slice of 0.45 nm thickness at the start of each nanosecond were used to calculate an averaged MSD until the next nanosecond (i.e, 50 frames for every ns). The diffusion coefficient for a given slice *z* was then determined by fitting the MSD values with the relation (here, dimensionality d=1):

$$D_z(z) = \lim_{t\to\infty} \frac{\langle |r(t) - r(0)|^2 \rangle}{2dt}$$

Potential of Mean Force Calculations
To calculate the PMF for pore formation, umbrella sampling simulations were performed. The chosen reaction coordinate was the distance between the center of mass of syb2 residues S115-T116, of all four SNARE complexes and the center of mass of stx1 residues F287-G288, again of all four SNARE complexes taken together. The starting structures for the first three windows was taken from the equilibrium simulation trajectories. The starting structures for next three umbrella sampling windows were then subsequently generated using steered molecular dynamics (SMD) simulations from the structure at the end of the previous umbrella sampling window. The SMD used a pull rate of -5x10^{-5} nm ps^{-1} and a force constant of 1000 kJ mol^{-1} nm^{-2}. The PMF was calculated over 15 independent windows along the reaction coordinate extending from an initial value of 6.2 nm up to 3.2 nm, with each window sampled over 250 ns to 300 ns and applying a harmonic potential with a force constant of 750 kJ mol^{-1} nm^{-2}. The first 100 ns of each window was discarded and a PMF profile was generated using the WHAM method in combination with the Bayesian bootstrapping method for error estimation, as implemented in GROMACS utility gmx wham.

The PMF for pore formation in a ~20 nm vesicle-bilayer system with a single SNARE complex was carried out using the distance between two hydrophilic probes as the reaction coordinate as described previously[12] (Supplementary Fig S6). The starting configurations for umbrella windows were obtained by pulling the probes along the z-axis, parallel to the bilayer normal, at a constant rate of -5 ×10^{-5} nm ps^{-1}. Separate pulling simulations were done for wt, syb2-KK and SNAP-25Δ9 SNARE complexes. For all simulations a harmonic force constant of 750 kJ mol^{-1} nm^{-2} was employed. From the pulling simulation, 16-20 umbrella windows were started to sample along the reaction coordinate. Each window was equilibrated for 300 ns.

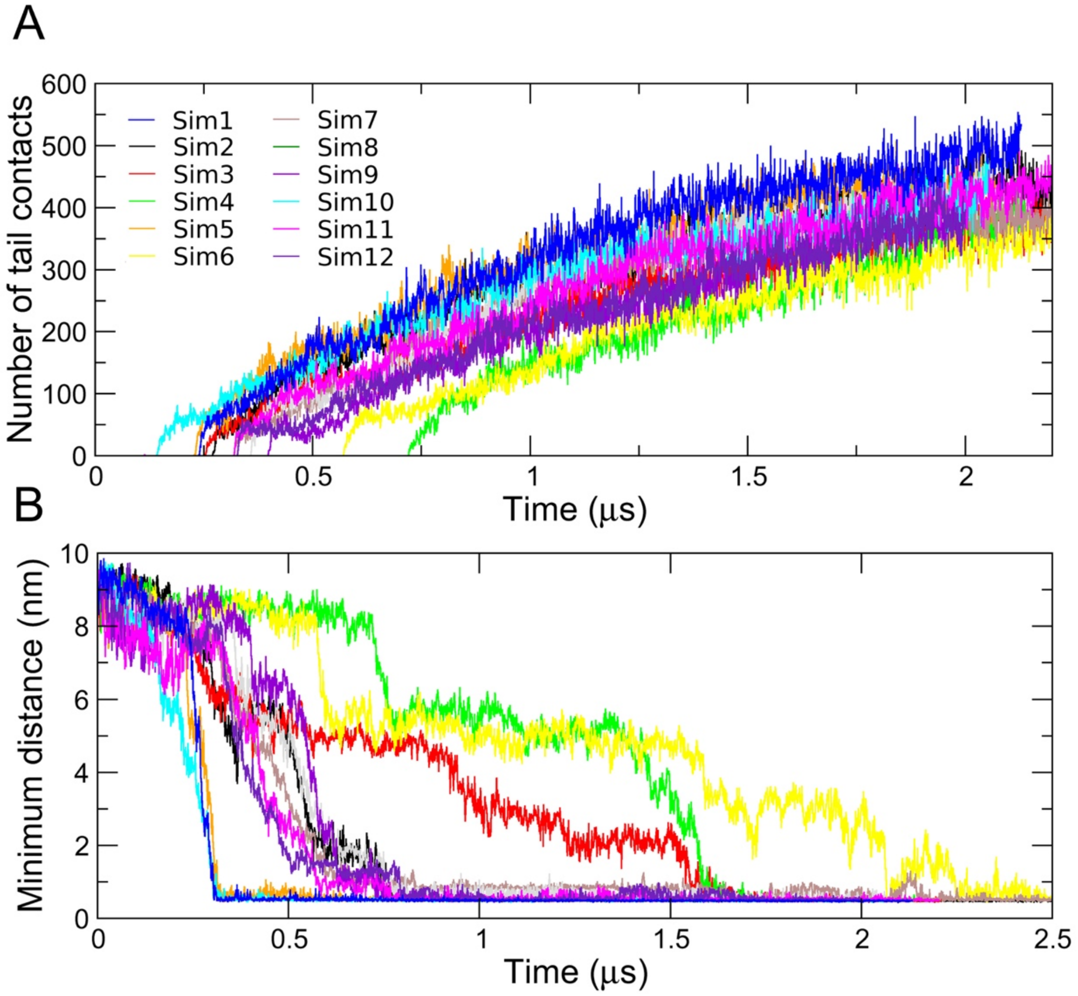

Fig. S1. Time course of lipid mixing of the two leaflets. (A) Contacts between the proximal leaflets of ND and bilayer from all simulations. **(B)** Minimum distance between phosphate groups of the distal leaflets of ND and the bilayer.

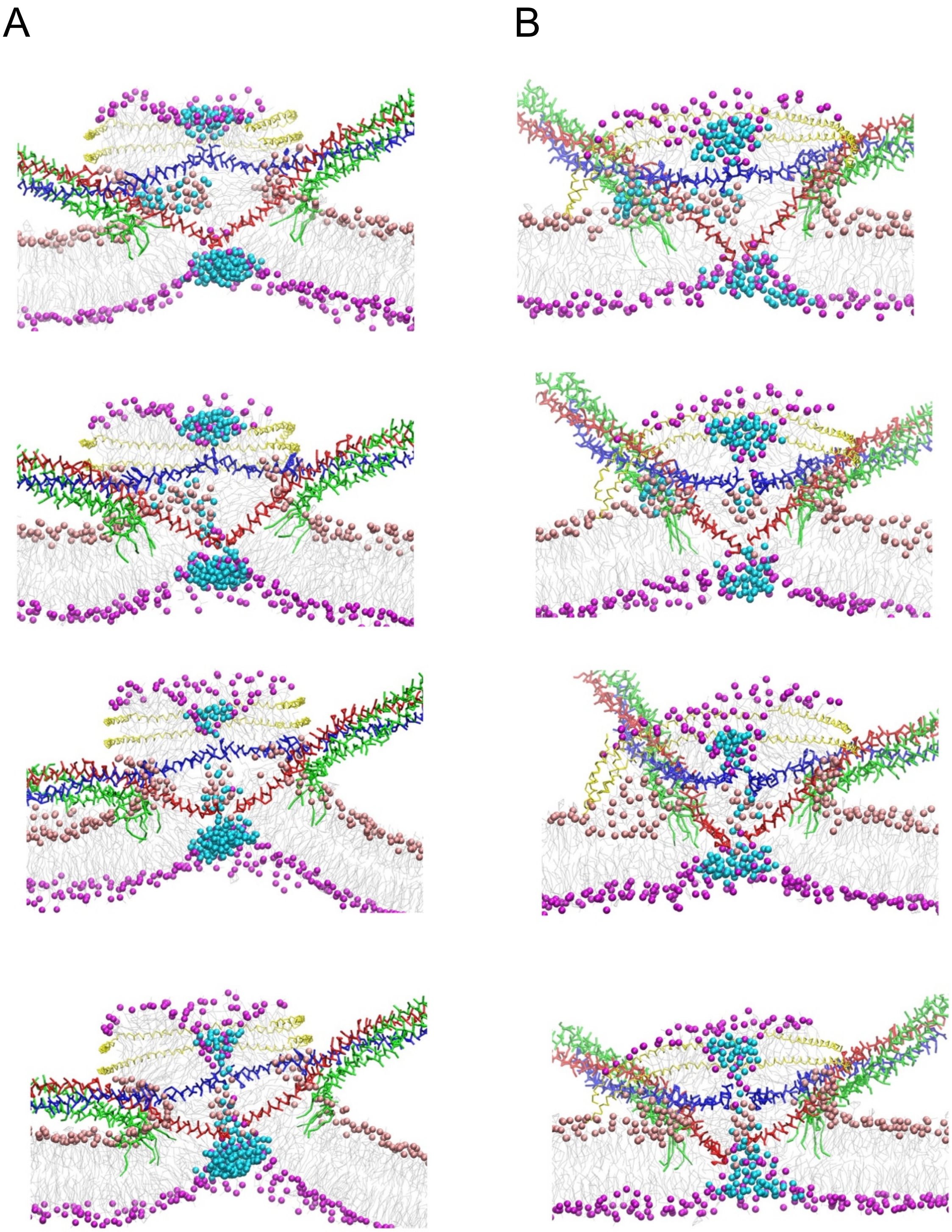

Fig. S2. Fusion pathways involving inverted H_{II} phase. (A) An elongated hexagonal phase (864 ns, top); an intermittent leaky pore (914 ns, middle top); rupture of leaky pore with the contents of inverted hexagonal phase fusing with distal leaflet (1197 ns, middle bottom); initiation of pore formation (1449 ns, bottom). The snapshots are taken from the simulation trajectory Sim3. **(B)** An elongated hexagonal phase (1704 ns, top); formation an inverted micelle (1983 ns, middle top); rupture of inverted micelle nucleating the fusion pore (2001 ns, middle bottom) and initiation of the fusion pore (2047 ns, bottom) in simulation Sim6. Note the close contact of the N-term residues of the SNARE TMDs with the waters trapped in the hexagonal phase (top panels in a and b). The water beads are colored cyan. The phosphate beads of proximal lipids are shown as pink spheres, while those of distal lipids are colored magenta. For clarity, only two of the SNARE complexes are shown along with the side chains in stick representations: Syb2 (blue), stx1 (red) and SNAP-25 (green).

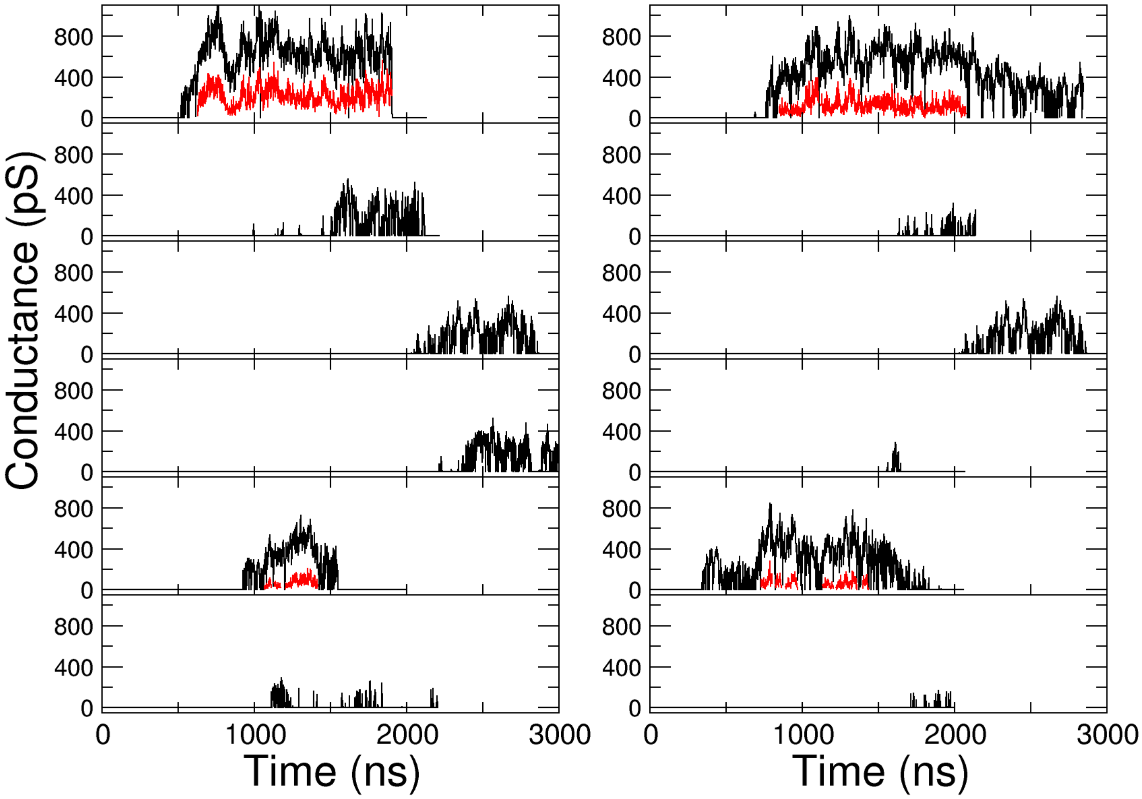

Fig. S3. Fusion pore conductance (in pS). Estimated conductances (black) calculated using equation 1 for all 12 simulations and diffusion-corrected pore conductances (red) calculated using equation 3 for trajectory segments where a continuous water density in the pore lasted for at least 25 ns.

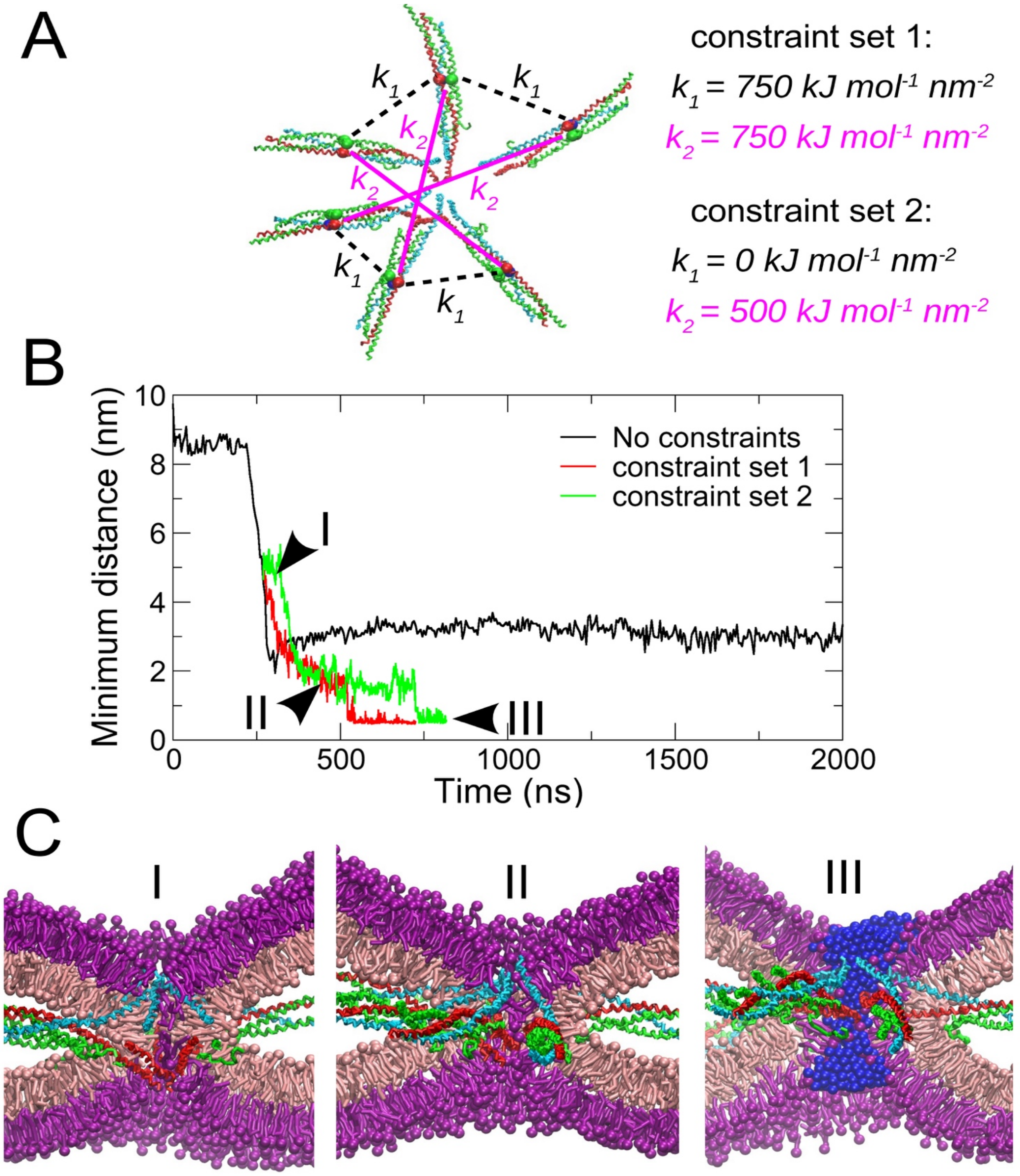

Fig. S4. Fusion in ~40 nm vesicle-bilayer system upon constraining the lateral diffusion of SNAREs. (A) Schematic of two sets of harmonic restraints (set 1 and set 2). The restrains were imposed on the distances between the center of mass of the backbone beads of layer 0 (shown as spheres) of different SNARE complexes. **(B)** Minimum distance between phosphate groups of the inner leaflet of the vesicle and the distal leaflet of bilayer when SNAREs were not constrained and allowed to diffuse freely (black). The distal leaflets fused to form a pore when constrained using harmonic restraints (set 1, red and set 2, green) **(C)** Snapshots at three different time points (marked by arrows in B, green trace) along the trajectory of the fusion pathway when SNAREs were constrained using set 2. Snapshot I (left) indicates the formation of initial contacts between the lipids from distal leaflets (shown in purple), and absence of an elongated H_{II} phase. This leads to further mixing of the distal lipids (II, middle) to form a non-leaky pore (III, right). In the right panel, only the waters inside the pore are shown (blue spheres).

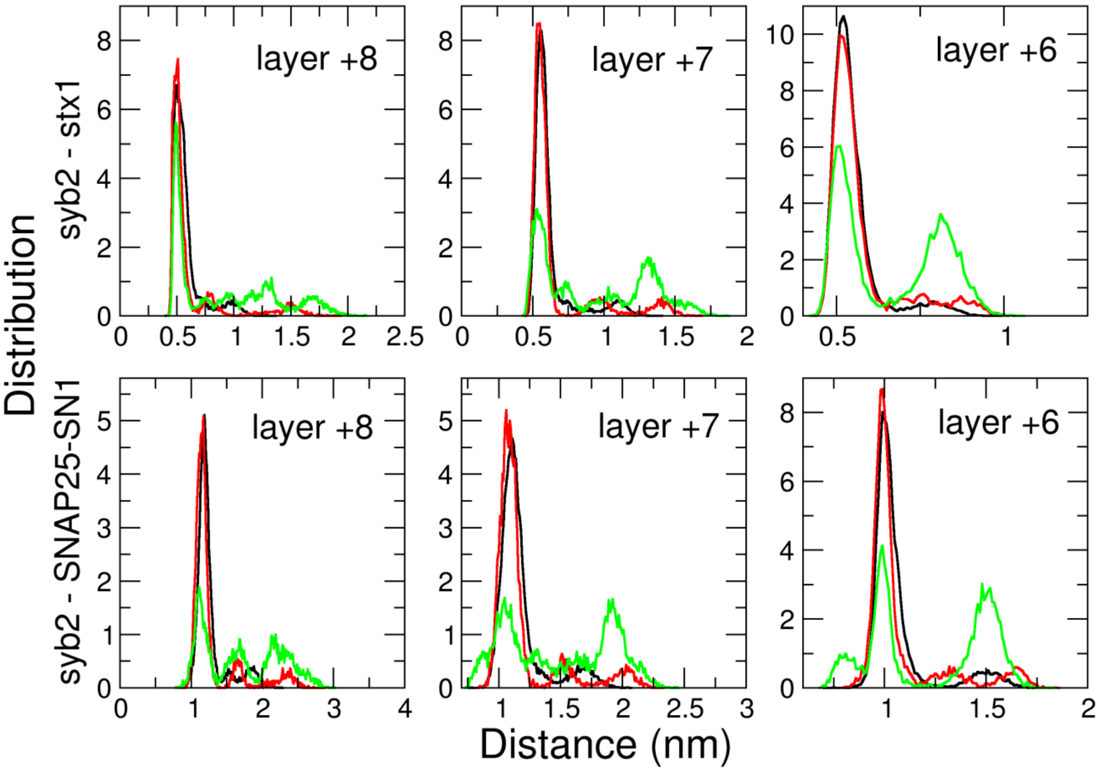

Fig. S5. Comparison of layer zippering of the SNARE complex in wild type, Syb2-KK and SNAP-25Δ9 mutants. Comparative distance distributions of the distances between the backbone beads of the residues of syb2 (84L, 81A, 77F) and stx1 (254A, 251T, 247A) that constitute the layers +8, +7 and +6 (top panels). Also shown are the distributions of the distances between the backbone beads of the residues of syb2 (84L, 81A, 77F) and SNAP-25-SN1 (81L, 78L, 74A) that constitute the layers +8, +7 and +6 (bottom panels). The distributions were calculated over last 500 ns for all simulations (Sim1 to Sim12) with the wild type SNARE complex (black), three simulations for syb2-KK mutant (red) and the three simulations for the SNAP-25Δ9 mutant (green).

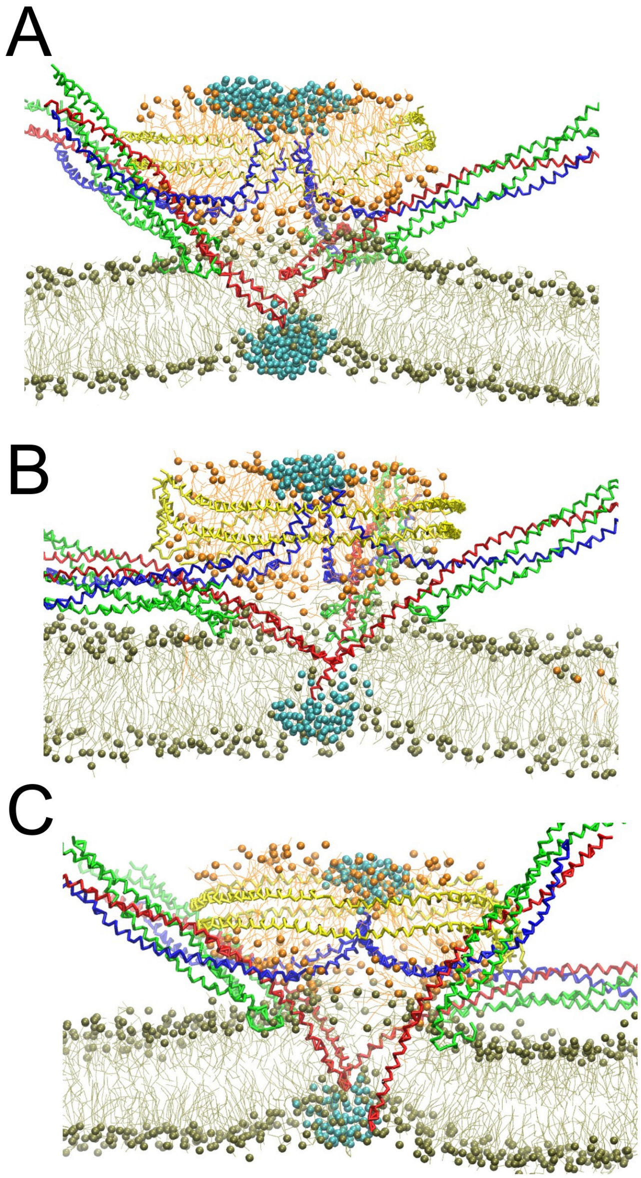

Fig. S6. Input structures for PMF calculation for the ND/bilayer setup. Starting configurations of **(A)** wt, **(B)** syb2-KK and **(C)** SNAP25-Δ9 SNARE complexes, corresponding to the reaction coordinate of 6.2 nm, for the free-energy calculations.

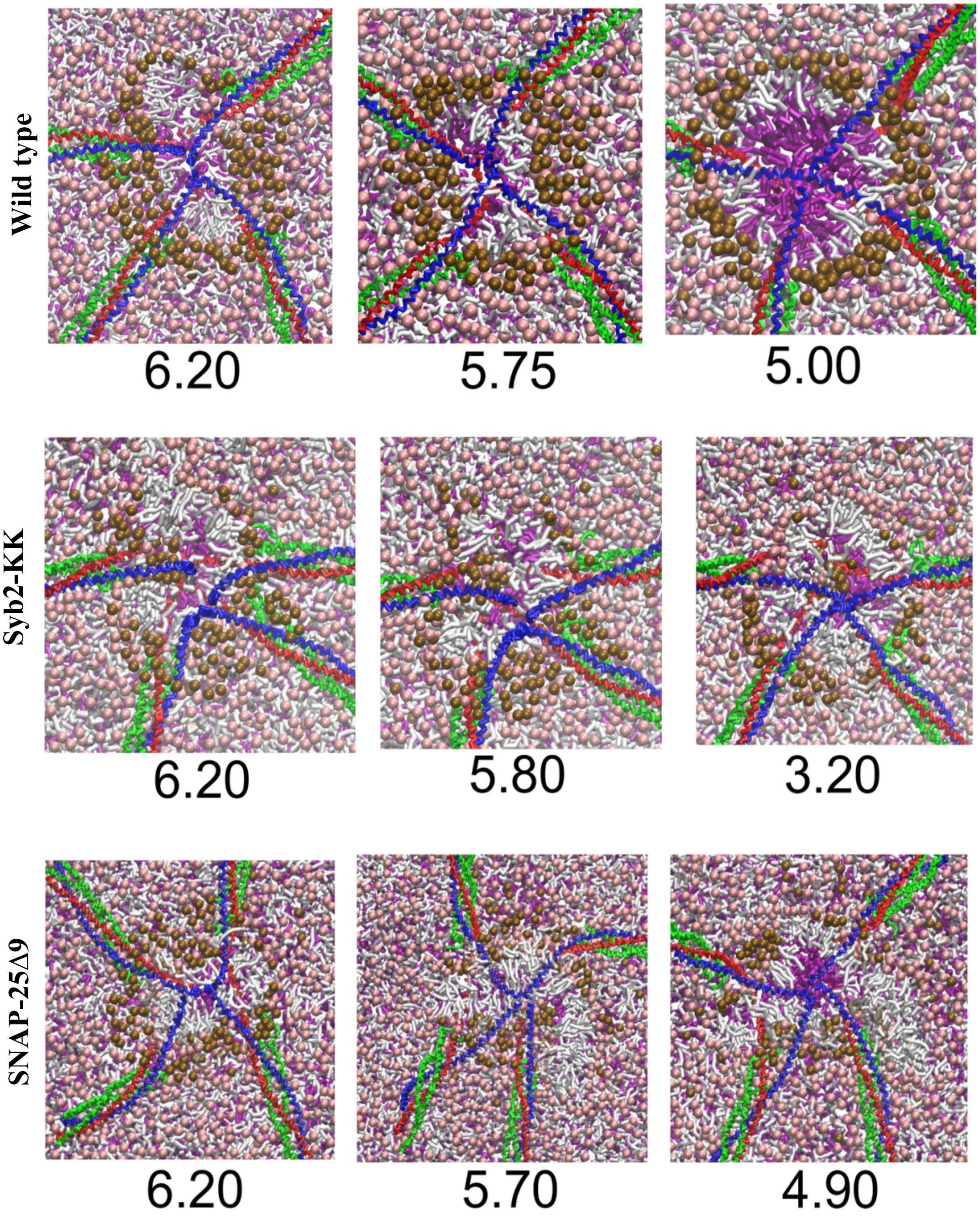

Fig. S7. Cross-section of stalk expansion in the ND-bilayer system in response to the pulling of the centers of mass of C-term residues of syb2 and stx1. Snapshots of the structures from the umbrella sampling windows from wt (top), syb2-KK (middle) and SNAP-25Δ9 from the umbrella sampling windows corresponding to the reaction coordinate values as labeled (in nm). The phosphate groups in the proximal leaflet of the bilayer are shown in pink with lipid tails in white. In addition, a few phosphate groups of the proximal leaflet of ND are shown as brown spheres to highlight the shape of the stalk. The lipids from the distal leaflet of the bilayer are shown in purple. Figures show that initially the stalk expands linearly followed by radial expansion. In both the mutants, the stalk elongates into an irregular shape simultaneously forming an elongated H_{II} phase. In the syb2-KK mutant, the H_{II} phase ruptures to form an inverted micelle intermediate (IMI). The IMI fuses with the distal leaflet of the bilayer (right panel, marked by brown spheres in the center), following a similar fusion pathway as shown in Supplementary Fig. S2B. No fusion pore was observed during the length of simulation (Fig. 6D in Main Text). In SNAP-25Δ9 mutant, a non-leaky pore was formed (Fig. 6E in Main Text), as also indicated by the indentation of lipids from distal leaflet (purple) of the bilayer (right), despite the presence of an H_{II} phase during the early stage. The H_{II} phase is pushed out by the approaching lipids from the distal leaflets, as the C-termini of syb2 and stx1 TMDs are pulled closer along the reaction coordinate.

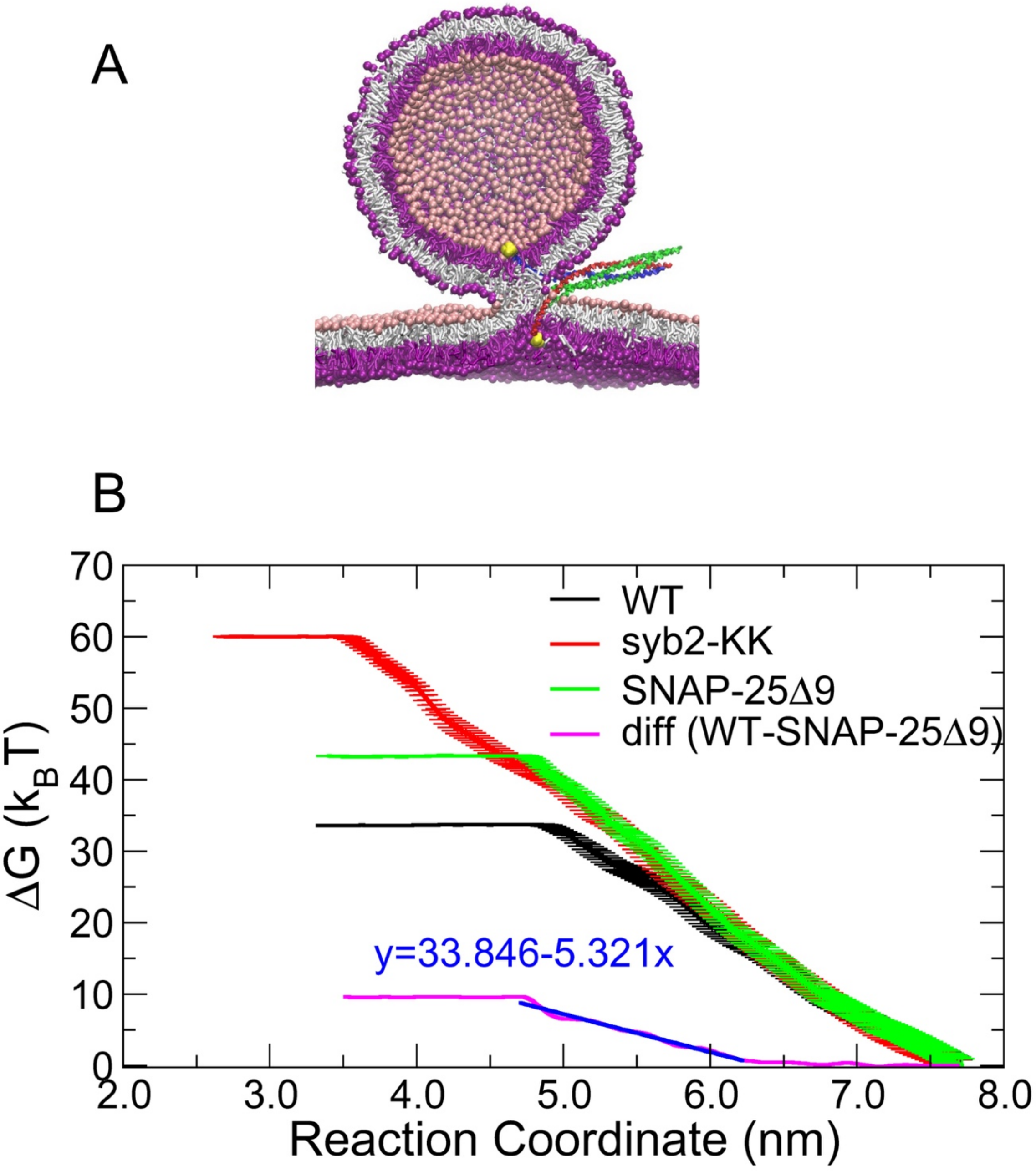
A
B
70
60
50
40
30
20
10
0
2.0
3.0
4.0
5.0
6.0
7.0
8.0
ΔG (k_BT)
Reaction Coordinate (nm)
WT
syb2-KK
SNAP-25Δ9
diff (WT-SNAP-25Δ9)
y=33.846-5.321x

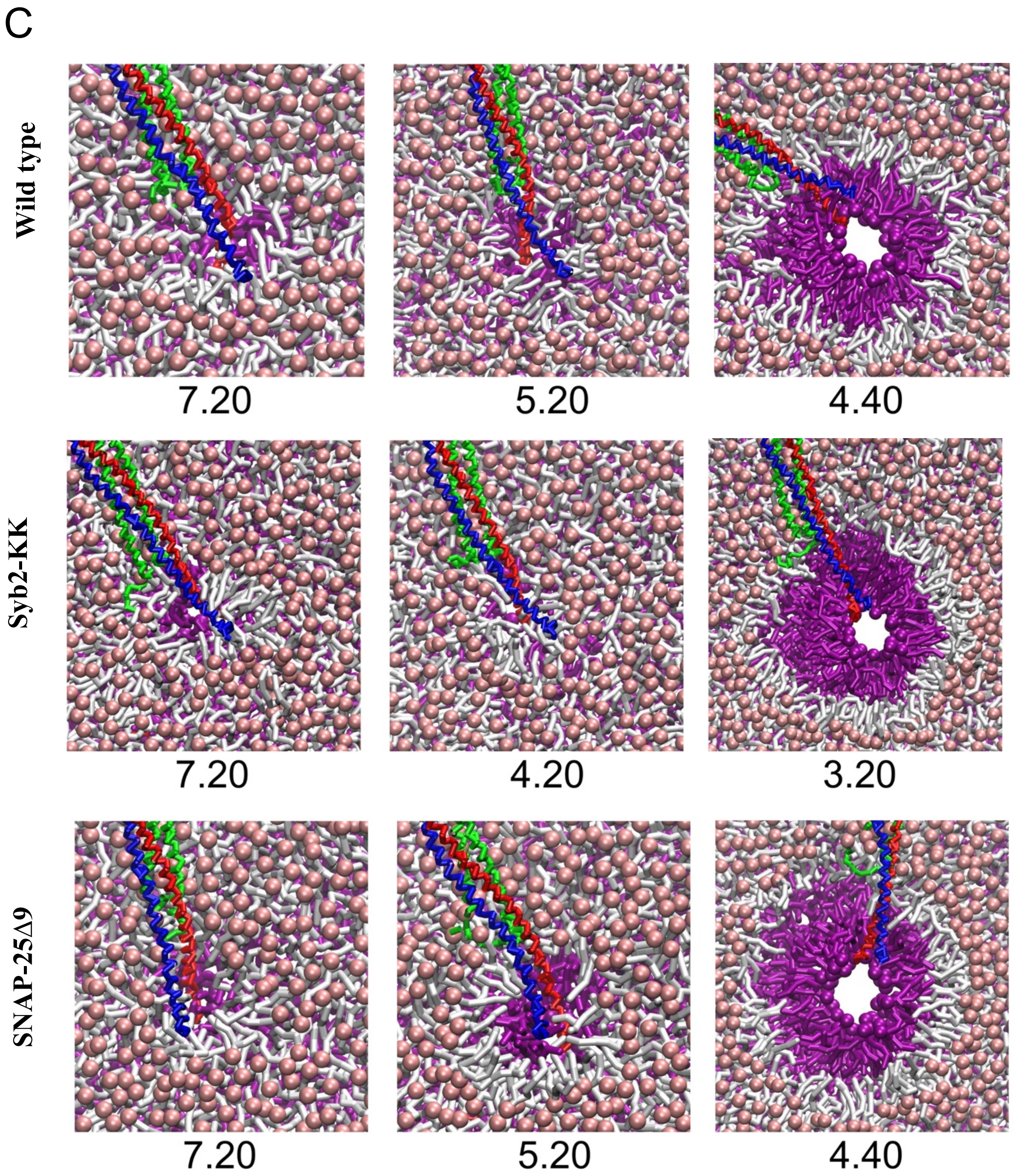

Fig S8. PMF profile for pore formation in a POPC vesicle-bilayer system with a single SNARE complex. (A) Illustration of the umbrella sampling simulation set-up, shown only for the wt SNARE. The reaction coordinate is defined as the distance, along z-axis, between the hydrophilic probes (yellow). **(B)** Free energy profile of pulling the probes through the stalk (left panel) for wt SNARE (black), syb2-KK (red) and SNAP-25Δ9 (green). The difference curve (magenta) was obtained by subtracting the energy profile for wt from that of the SNAP-25Δ9 mutant. A straight line fit through the difference curve in the indentation regime (6.7 nm to 4.2 nm) with a slope of ~5.3 kT nm^{-1} indicates that the force exerted by SNAP-25Δ9 on the stalk is weakened by ~20 pN in comparison to wt SNAP-25. **(C)** Cross section of the stalk expansion from the umbrella sampling windows from wt (top), syb2-KK (middle) and SNAP-25Δ9 corresponding at the reaction coordinate as labeled (in nm), illustrating the regular expansion of the stalk and formation of a non-leaky pore in all cases.

Table S1. Lipid composition of plasma membrane model. The lipid composition of the bilayer is based on the lipid composition of rat brain synaptosomal plasma membrane[1]. All values are shown in percentages. The numbers in brackets represent the percentage of each lipid species with respect to the total number of phospholipids. Note that some lipids are shown to have two fatty acid chains at the same sn-position, as they are same at the level of martini CG resolution. (IC: intracellular; EC: extracellular).

Lipids			**Before self-assembly (%)**		**After self-assembly (%)**	
sn-1	sn-2	Count	IC leaflet	EC leaflet	IC leaflet	EC leaflet
Phosphatidylcholine (PC)		(41%)				
16:0/18:0	16:0/18:0	437	0	100	24	76
16:0/18:0	18:1	486	0	100	29	71
16:0/18:0	20:4/22:4	99	0	100	25	75
16:0/18:0	22:5/22:6	60	0	100	20	80
Phosphatidylethanolamine (PE)		(34%)				
16:0/18:0	18:1	112	100	0	67	33
16:0/18:0	20:4/22:4	296	100	0	69	31
16:0/18:0	22:5/22:6	114	100	0	76	24
22:5/22:6	22:5/22:6	367	100	0	72	28
Phosphatidylserine (PS)		(13%)				
16:0/18:0	18:1	52	100	0	58	42
16:0/18:0	20:4/22:4	39	100	0	74	26
16:0/18:0	22:5/22:6	252	100	0	71	29
Sphingomyelin (SM)		(5%)				
16:0/18:0	16:0/18:0	120	0	100	23	78
16:0/18:0	23:1/24:1	3	0	100	33	67
20:0/22:0	20:0/22:0	8	0	100	0	100
24:0	24:0	3	0	100	0	100
Phosphatidylinositol (PI)		(3%)				
16:0/18:0	18:1	16	100	0	69	31
16:0/18:0	20:4/22:4	68	100	0	72	28
16:0/18:0	22:5/22:6	8	100	0	75	25
Glycolipid 1 (GM1)		(2%)				
16:0/18:0	16:0/18:0	52	0	1	12	88
Glycolipid 3 (GM3)		(2%)				
16:0/18:0	16:0/18:0	52	0	1	15	85
Cholesterol		(43%) 1140	0	1		

Table S2. Lipid composition of the nanodisc. The experimental values are obtained from the lipid composition of synaptic vesicle membranes[2]. (IV: intravesicular; CP: cytoplasmic).

			Asymmetry (%)	
Lipids	**Exptl. (%)**	**Nanodisc (%)**	IV leaflet	CP leaflet
POPC	36.1	35.2	81	19
POPE	41.9	45.4	27	73
POPS	12.3	12.8	32	68
DPSM	7.4	6.6	77	23
CHOL	81.0	78.6	53	47

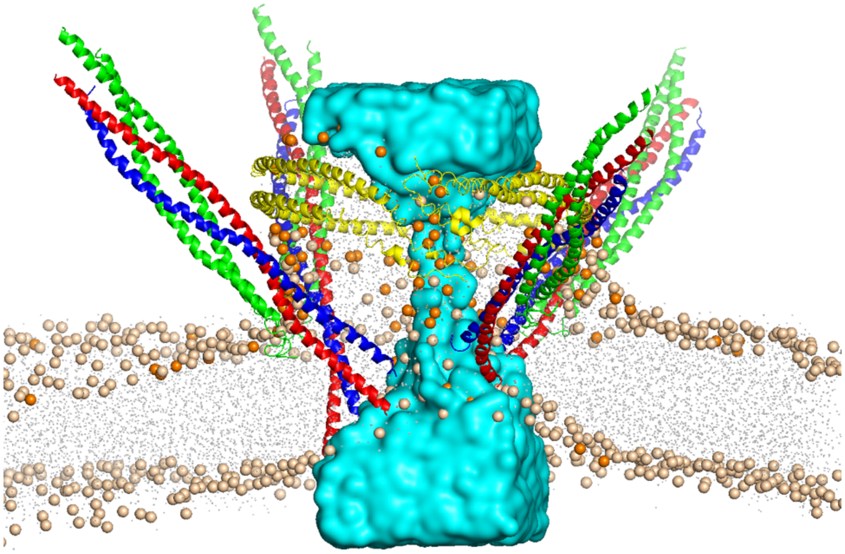

Movie S1. Fusion pore formation between a nanodisc and a bilayer. Coarse-grained simulation trajectory (Sim1, 2.1 μs) of membrane fusion, pore formation and its subsequent closure. Water density at the fusion site is shown as cyan surface.

References

1 Stein, A., Weber, G., Wahl, M. C. & Jahn, R. Helical extension of the neuronal SNARE complex into the membrane. *Nature.* **460** (7254), 525-528, (2009).

2 Sali, A. & Blundell, T. L. Comparative protein modelling by satisfaction of spatial restraints. *Journal of Molecular Biology.* **234** (3), 779-815, (1993).

3 Roy, A., Kucukural, A. & Zhang, Y. I-TASSER: a unified platform for automated protein structure and function prediction. *Nat Protoc.* **5** (4), 725-738, (2010).

4 Sharma, S., Kim, B. N., Stansfeld, P. J., Sansom, M. S. & Lindau, M. A Coarse Grained Model for a Lipid Membrane with Physiological Composition and Leaflet Asymmetry. *PLoS One.* **10** (12), e0144814, (2015).

5 Denisov, V. P., Schlessman, J. L., Garcia-Moreno, E. B. & Halle, B. Stabilization of internal charges in a protein: water penetration or conformational change? *Biophysical Journal.* **87** (6), 3982-3994, (2004).

6 Borhani, D. W., Rogers, D. P., Engler, J. A. & Brouillette, C. G. Crystal structure of truncated human apolipoprotein A-I suggests a lipid-bound conformation. *Proceedings of the National Academy of Sciences, USA.* **94** (23), 12291-12296, (1997).

7 Takamori, S. *et al.* Molecular anatomy of a trafficking organelle. *Cell.* **127** (4), 831-846, (2006).

8 Bayburt, T. H., Grinkova, Y. V. & Sligar, S. G. Assembly of single bacteriorhodopsin trimers in bilayer nanodiscs. *Archives of Biochemistry and Biophysics.* **450** (2), 215-222, (2006).

9 Siuda, I. & Tieleman, D. P. Molecular Models of Nanodiscs. *J Chem Theory Comput.* **11** (10), 4923-4932, (2015).

10 Khelashvili, G. & Harries, D. How cholesterol tilt modulates the mechanical properties of saturated and unsaturated lipid membranes. *Journal of Physical Chemistry B.* **117** (8), 2411-2421, (2013).

11 Smart, O. S., Coates, G. M., Sansom, M. S., Alder, G. M. & Bashford, C. L. Structure-based prediction of the conductance properties of ion channels. *Faraday Discussions.* **111** 185-199, (1999).

12 Risselada, H. J., Bubnis, G. & Grubmuller, H. Expansion of the fusion stalk and its implication for biological membrane fusion. *Proc Natl Acad Sci U S A.* **111** (30), 11043-11048, (2014).